

The fractal dimension of star-forming regions at different spatial scales in M33

Néstor Sánchez¹, Neyda Añez², Emilio J. Alfaro¹, Mary Crone Odekon³

nestor@iaa.es

ABSTRACT

We study the distribution of stars, HII regions, molecular gas, and individual giant molecular clouds in M33 over a wide range of spatial scales. The clustering strength of these components is systematically estimated through the fractal dimension. We find scale-free behavior at small spatial scales and a transition to a larger correlation dimension (consistent with a nearly uniform distribution) at larger scales. The transition region lies in the range $\sim 500 - 1000$ pc. This transition defines a characteristic size that separates the regime of small-scale turbulent motion from that of large-scale galactic dynamics. At small spatial scales, bright young stars and molecular gas are distributed with nearly the same three-dimensional fractal dimension ($D_{f,3D} \lesssim 1.9$), whereas fainter stars and HII regions exhibit higher values $D_{f,3D} \simeq 2.2 - 2.5$. Our results indicate that the interstellar medium in M33 is on average more fragmented and irregular than in the Milky Way.

Subject headings: galaxies: individual: M33 — galaxies: structure — stars: formation

1. Introduction

In the Milky Way, gas and dust are organized in a hierarchical and self-similar manner that it is supposed to be a consequence of turbulent processes (Elmegreen & Scalo 2004).

¹Instituto de Astrofísica de Andalucía, CSIC, Apdo. 3004, E-18080, Granada, Spain.

²Departamento de Física, Facultad de Ciencias, Universidad del Zulia, Maracaibo, Venezuela.

³Department of Physics, Skidmore College, Saratoga Springs, NY 12866, USA.

These fractal patterns are observed over at least the range $0.1 \lesssim r \lesssim 100$ pc, going from dense cores to giant molecular clouds (GMCs, Bergin & Tafalla 2007). The formation of stars also shows fractal features, usually observed in regions with a spatial hierarchy ranging from a few pc up to about a kpc for so-called star complexes (e.g. Efremov 1995; Elmegreen 2010). Star clusters are in the lower levels of this hierarchy, although there is evidence that young open clusters also exhibit smaller substructure (Schmeja et al. 2008; Sánchez & Alfaro 2009).

This complexity can be characterized in many different ways. Some common strategies, such as estimating mass or size distributions of certain types of objects (clouds, cores, clusters), have to be taken with extreme caution because they depend, among other things, on the criteria adopted to define the objects (Pineda et al. 2009; Curtis & Richer 2010). Note that in a rigorously hierarchical scenario there is no characteristic spatial scale that can be used to define any particular structure. Moreover, it has been shown that projection effects can significantly alter the estimated masses and sizes of molecular clouds (Sánchez et al. 2006; Shetty et al. 2010). Many other tools are now widely used to describe the complexity of these structures objectively and quantitatively (see Elmegreen & Scalo 2004, for a comprehensive review). Fractal analysis is particularly appropriate for dealing with hierarchical and self-similar systems. The fractal dimension D_f , which quantifies the spatial heterogeneity, can be calculated for both the distribution of gas and the distribution of star-forming sites. This approach allows for the comparison of similar objects in different regions and/or under different physical conditions, and also the comparison of different types of objects.

It is often accepted that the fractal dimension observed in the interstellar medium (ISM) has a nearly universal value around $D_f \simeq 2.3 \pm 0.3$ (e.g. Elmegreen & Falgarone 1996). This universality would indicate either that interstellar turbulence is driven by the same physical mechanisms everywhere, or that different physical mechanisms can (and tend to) generate essentially the same type of structures. However, the robustness of this conclusion is questionable given the wide variety of results reported and their associated uncertainties. If D_f is inferred from properties such as cloud masses or sizes, the resulting uncertainties may be unacceptably large (Sánchez et al. 2006). A more appropriate strategy is to measure the fractal dimension directly from an observed map. The boundaries of the projected images of interstellar clouds in the Galaxy have fractal dimension values spread over the range $1.2 \lesssim D_{\text{per}} \lesssim 1.5$ (Sánchez et al. 2005) but it is not clear whether there are real variations from region to region or whether the different values reflect different observational data and/or analysis techniques. Moreover, even though $D_{\text{per}} \simeq 1.3$ is a constant, the assumption that one can relate D_{per} to the fractal dimension in three dimensions using $D_f = D_{\text{per}} + 1 \simeq 2.3$ has been shown not to be valid (Sánchez et al. 2005).

In a previous work we analyzed several emission maps of three different molecular clouds (Ophiuchus, Perseus and Orion) and obtained $D_f \simeq 2.6 \pm 0.1$ with no evidence of significant variations (Sánchez et al. 2007b). Similar fractal patterns should be observable in the distribution of newborn stars if the distribution of high-density cores follows the spatial structure of the parental cloud. In fact, the young massive stars in the Gould Belt exhibit a fractal pattern with the similar value $D_f = 2.68 \pm 0.04$ (Sánchez et al. 2007a). However, a recent study by Schneider et al. (2010) reports remarkable differences in the Δ -variance spectra between low-mass star forming clouds and massive GMCs. Star clusters also show a wide variety of spatial patterns even for young, embedded clusters (Lada & Lada 2003; Cartwright & Whitworth 2004; Schmeja et al. 2008), but it is not clear whether these variations are due to evolution or to differences in the structure of the original clouds (Goodwin & Whitworth 2004; Schmeja & Klessen 2006; Allison et al. 2009).

Simulations of turbulent fluids produce very different structures depending on which processes are considered in the system. For example, Federrath et al. (2009) showed that simulations of supersonic isothermal turbulence in the extreme case of purely compressive energy injection, produce a significantly smaller fractal dimension for the density distribution ($D_f \sim 2.3$) than in the case of purely solenoidal forcing ($D_f \sim 2.6$). Although it is widely accepted that turbulence is the primary driver of the structure and motion of the ISM, the main energy sources for this turbulence are not yet well established. Part of the problem lies in the wide variety of physical processes that can generate turbulent motions, such as protostellar jets and outflows, (proto)stellar winds and ionizing radiation, expanding HII regions, supernovae, cloud collisions, galaxy interactions, and gravitational, magnetorotational and other fluid instabilities (recent reviews on interstellar turbulence can be seen in Elmegreen & Scalo 2004; Mac Low & Klessen 2004; Burkert 2006; McKee & Ostriker 2007). It is reasonable to expect that, depending on the dominant physical mechanisms driving the turbulence, the resulting structure may differ from region to region in the Galaxy.

A related issue is the spatial extent of this self-similar behavior, since different physical mechanisms might dominate on different scales. In the solar neighborhood, fractal behavior has been observed for the distribution of young open cluster and young stars at spatial scales of up to ~ 1 kpc (de La Fuente Marcos & de La Fuente Marcos 2006; Sánchez et al. 2007a; de la Fuente Marcos & de la Fuente Marcos 2009). In external galaxies, hierarchical structures extend up to $\gtrsim 1$ kpc scales for the gas and for stars and star-forming sites (some recent examples are in Bastian et al. 2007; Dutta et al. 2008; Gieles et al. 2008; Odekon 2008; Sánchez & Alfaro 2008; Bastian et al. 2009; Dutta et al. 2009b; Scheepmaker et al. 2009; Bonatto & Bica 2010). Some galaxies show a change in clustering strength with scale. This has been seen in both gas (Elmegreen et al. 2001; Padoan et al. 2001; Kim & Park 2007; Dutta et al. 2008, 2009a) and young stars (Odekon 2008). There is also evidence for

variations among galaxies. Recent work indicates that the power spectrum of the gas distribution is steeper for galaxies with a larger star formation rate per unit area (Willett et al. 2005; Dutta et al. 2009b). This trend is consistent with the claim that bright galaxies tend to distribute their star-forming sites in less clustered patterns (Parodi & Binggeli 2003; Odekon 2006; Sánchez & Alfaro 2008). In other words, a larger star formation rate in a galaxy tends to be correlated with a larger fractal dimension. Thus, at least on galactic spatial scales, a universal picture for the fractal properties does not seem to hold.

A significant challenge in interpreting different measurements is that authors present fractal dimensions for different ranges of scales, identify their samples in different ways, and make different assumptions regarding the comparison between two-dimensional measures of clustering strength and the implications for the actual three-dimensional structure. Our approach here is to consider a case study in which we systematically analyze the clustering of different components of a single galaxy over a wide range of spatial scales. Because of its proximity, large size, and low inclination, M33 is a suitable object for this task. Bastian et al. (2007) showed that the star formation in this galaxy appears to be inherently hierarchical, with no characteristic size for star-forming regions. However, Odekon (2008) found a transition on a scale of several hundred pc in the slope of the autocorrelation function for young stars. In this work, we study the clustering strength in the distribution of young stars, HII regions, molecular gas, and individual giant molecular clouds. Treating each of these components as consistently as possible, we can directly compare the clustering strength of each component as a function of scale. In addition, we examine in detail the steepness of the transition in clustering strength, evaluate the range of scales over which it occurs, and analyze its meaning in the context of the maximum spatial scale of coherent star formation. We apply robust algorithms that have been previously developed and tested on real data and simulated fractals. Section 2 describes the data and Section 3 describes our calculation of the fractal dimensions. An analysis and discussion of the results are presented in Section 4. Finally, a summary and the main conclusions are given in Section 5.

2. The data

The catalog of Massey et al. (2006), available via the VizieR¹ database, provides *UBVRI* photometry of 146,622 stars in M33 down to apparent magnitudes of 23 with photometric errors less than 10%. From this catalog we use the same set of young stars (ages $\lesssim 30$ Myr) that Odekon (2008) used to calculate the angular two-point autocorrelation function, that is,

¹<http://vizier.u-strasbg.fr>

stars fulfilling the criteria $-0.3 \leq V - I \leq 0.0$ and $-6.0 \leq M_I \leq -4.0$. This set of stars was divided into two subsets that we refer to simply as “bright” stars ($-0.3 \leq V - I \leq -0.1$ and $-6.0 \leq M_I \leq -5.0$) and “faint” stars ($-0.3 \leq V - I \leq 0.0$ and $-4.5 \leq M_I \leq -4.0$). The total numbers of stars for the bright and faint sets are 534 and 1644, respectively. For the HII regions we use the catalog of Hodge et al. (1999), which gives the positions of 1272 HII regions in M33. From this total data set, we remove regions classified as unresolved, diffuse, linear and/or any other factor that may raise doubts on the real nature of such regions. We also remove the regions having null integrated H α fluxes in the catalog. This means that we only consider regions having an isophote level of at least $10^{-16} \text{ erg s}^{-1} \text{ cm}^{-2} \text{ arcsec}^{-2}$. With these requirements the total number of “bright” HII regions to consider is 617. The distribution of giant molecular clouds in M33 is obtained from the catalog of Rosolowsky et al. (2007) (also available through Vizier) from which we extract the positions of 149 GMCs.

We adopt a position angle of 23 degrees and an inclination of 55 degrees (taken from Hyperleđa²) to deproject the positions of stars, HII regions and GMCs. This is a first step necessary to avoid the calculated fractal dimension becoming smaller than its true value (Sánchez & Alfaro 2008). To convert the angular sizes into linear sizes, we assume a distance of 960 kpc (Bonanos et al. 2006; U et al. 2009). The positions of bright stars, HII regions and GMCs relative to the galactic center ($\alpha_{J2000.0} = 1^{\text{h}}33^{\text{m}}51^{\text{s}}$, $\delta_{J2000.0} = +30^{\circ}39'37''$) are shown in Figure 1.

As an additional way to study the the distribution of molecular gas, we also directly use the high resolution maps of CO ($J = 1 \rightarrow 0$) emission for the center region of M33, kindly provided by Erik Rosolowsky (Rosolowsky et al. 2007). To avoid problems that might arise when estimating the fractal properties in noisy maps (Sánchez et al. 2007b), we use only the combined NRO+BIMA+FCRAO data cube which has the highest signal-to-noise ratio. The noise varies across the map but the typical rms noise temperature is 60 mK (Rosolowsky et al. 2007). The final resolution is 20" (93 pc). We collapse the data cube to produce the map of integrated intensity of CO emission shown in Figure 2.

3. Estimation of the fractal dimension

The degree of clustering of a point distribution can be quantified by the correlation dimension D_c . For scale-free sets, this can be calculated from $C(r) \sim r^{D_c}$, where the correlation integral $C(r)$ is the average number of stars within a distance r of each star. In practice, the distribution of stars is not truly scale-free. For example, Odekon (2008) found

²<http://leda.univ-lyon1.fr>

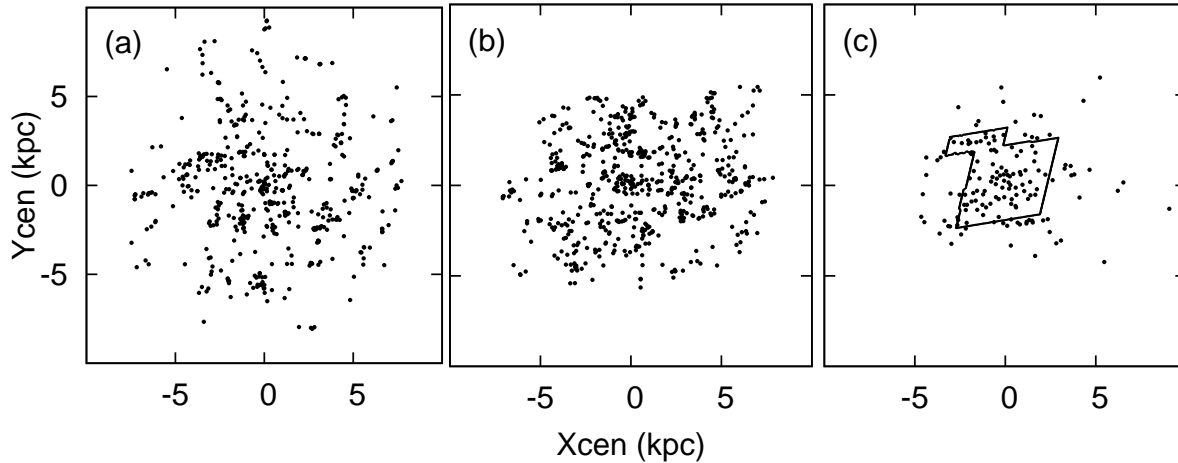


Fig. 1.— Spatial distributions of (a) bright stars, (b) bright HII regions and (c) GMCs in M33. The axis coordinates are positions relative to the galactic center in kpc. The inset in panel (c) shows the area corresponding to the molecular gas map (Fig. 2).

a transition in the clustering strength of young stars in M33 at a scale of about 300 pc. Because the correlation integral for any particular scale r includes information about the clustering on all scales less than r , any deviation from a scale-free distribution will affect, to some degree, the form of $C(r)$ on scales larger than the deviation. For this reason, it is sometimes preferable to use the differential form $c(r)$, where $C(r) \sim \int_0^r c(r')dr'$, especially if the goal is to determine the scale at which a change in clustering strength takes place. Because of its differential nature, however, $c(r)$ is too messy for small data sets.

Another reason the distribution of stars is not actually scale-free is the finite size of a galaxy. For an otherwise scale-free distribution with a well-defined edge, one approach to dealing with this limitation is to include, for each scale r , only those stars at least r from the edge. Sánchez et al. (2007a) used the minimum-area convex polygon that contains all the points of finite two-dimensional fractal distributions, and showed that it is an effective way of performing an edge correction. We use this method to create an edge-corrected version for $C(r)$. Finally, on small scales the observed distribution of stars is not scale-free because of resolution limits and, ultimately, because of the size of the stars themselves. Sánchez et al. (2007a) found that the calculation of $C(r)$ for two-dimensional fractals is reliable on scales for which the standard deviation of $C(r)$ is not greater than $C(r)$ itself. We use this as our guide in determining the smallest scales to include in our fits to the data.

Figure 3 shows our results for correlation integral $C(r)$ and the differential form $c(r)$

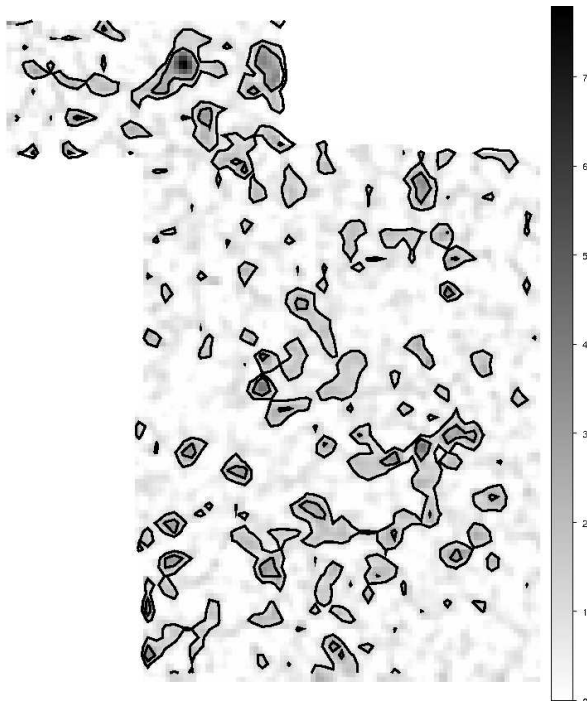


Fig. 2.— Integrated intensity of CO emission in the central region of M33 (Fig. 1). The gray scale runs linearly from 0 (white) to the maximum value (black, $\sim 7.8 \text{ K km s}^{-1}$). Contour levels are shown at 1 and 2 K Km s^{-1} .

for each type of point distribution in our sample: bright stars, faint stars, HII regions, and GMCs. Each panel includes three functions; from top to bottom, they are the edge-corrected correlation integral $C(r)/r^2$, the uncorrected version of $C(r)/r^2$, and the differential correlation function $c(r)/r$. The functions are normalized so that a random two-dimensional distribution (corresponding to $D_c = 2$) would produce a horizontal line. In other words, the slope on the log-log plot is $D_c - 2$, so that a more strongly clustered distribution decreases more quickly with scale. A comparison of the bottom two functions in each panel illustrates the fact that the differential form $c(r)$ is more sensitive to changes with scale, but messier, than the integral form $C(r)$. A comparison of the top two function in each panel illustrates the effect of the edge-correction algorithm, flattening the slope on large scales.

Gray shaded line segments in Figure 3 show our power law fits to the edge-corrected $C(r)$. Following Sánchez et al. (2007a) and Sánchez & Alfaro (2008), the range in r used for the fits is limited on small scales to regions where the variation in $C(r)$ is not greater than $C(r)$ itself; these lower limits are $\sim 100 \text{ pc}$ for stars and HII regions and $\sim 450 \text{ pc}$ for GMCs. In order to consider the possibility of a transition in D_c , we performed separate fits at large and small scales. The range of spatial scales for the transition was varied and the result that

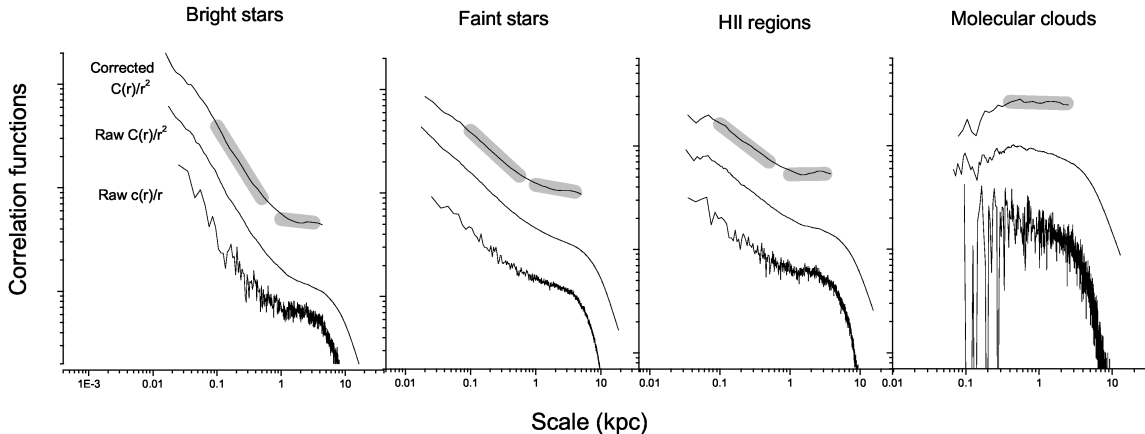


Fig. 3.— From top to bottom in each panel, the edge-corrected correlation integral $C(r)/r^2$, the raw correlation integral $C(r)/r^2$, and the differential correlation function $c(r)/r$ for the distributions of pointlike objects. The data have been arbitrarily shifted vertically for clarity. Shaded line segments show power-law fits.

minimizes the sum of the squared residuals, is that shown in Figure 3 and listed in Table 1. We calculated uncertainties in D_c , also listed in Table 1, using a bootstrap algorithm.

All of the objects except the GMCs exhibit scale-free clustering on small scales and a clear transition to a flatter slope near 1 kpc. The transition region is found to lie in the range $500 \lesssim r \lesssim 1000$ pc for bright stars and $600 \lesssim r \lesssim 950$ for faint stars and HII regions.

We use a very different type of clustering measure on the projected CO emission map (Fig. 2). For these data, we calculated the perimeter-based dimension D_{per} using the same algorithm as in Sánchez et al. (2005). We chose brightness levels from the lowest to the highest values in steps of 0.5 K Km s^{-1} . At each brightness level the algorithm defines “objects” in the image as sets of connected pixels whose brightness value is above this level. Then, the perimeters P and areas A of each object are determined and the perimeter dimension is obtained from the relation $P \sim A^{D_{\text{per}}/2}$. We did not consider objects containing less than 20 pixels because most of the structural details are lost in objects this small (Sánchez et al. 2005). For the same reason we also excluded objects touching the edge of the map. The perimeter-area log-log plot is shown in Figure 4 and the resulting perimeter dimension (twice the slope of the best fit) is also listed in Table 1. The maximum spatial scale involved in this calculation can be estimated as $\sqrt{A_{\text{max}}}$, being A_{max} the area of the largest projected cloud in the map. We obtained $A_{\text{max}} = 240 \text{ pixel}^2$ and the pixel size is 6.87 arcsec (Rosolowsky et al. 2007), then the maximum size is ~ 500 pc.

Table 1 summarizes the fractal dimensions calculated for each type of data. The 2D

Table 1. Summary of Calculated Fractal Dimensions for M33

Sample	N_{dat}	Small spatial scales ^a		Large spatial scales	
		$D_{f,2D}$ ^b	$D_{f,3D}$	$D_{f,2D}$	$D_{f,3D}$
Bright stars	534	1.01 ± 0.05	1.0-1.9	1.93 ± 0.03	2.8-2.9
Faint stars	1644	1.42 ± 0.04	2.2-2.4	1.89 ± 0.02	2.8-2.9
HII regions	617	1.48 ± 0.08	2.3-2.5	2.01 ± 0.03	2.9-3.0
Molecular clouds	149	1.98 ± 0.04	2.8-3.0
CO emission map	...	1.65 ± 0.06	1.6-1.8

^aFor bright and faint stars and HII regions small spatial scale means $\lesssim 500$ pc and large scale means $\gtrsim 1$ kpc. For molecular gas large scale is $\gtrsim 500$ pc (distribution of clouds) and small scale is $\lesssim 500$ pc (CO map).

^b $D_{f,2D}$ refers either to the two-dimensional correlation dimension D_c (for the distribution of stars, HII regions and GMCs) or to the perimeter-area based dimension D_{per} (for the CO map). $D_{f,3D}$ is the corresponding three-dimensional fractal dimension.

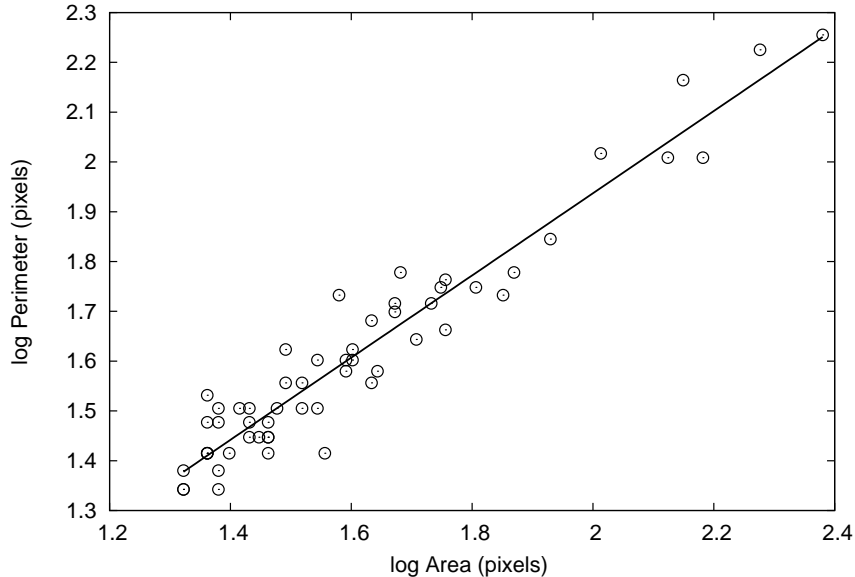


Fig. 4.— Perimeter as a function of the area for objects in the CO emission map (Fig. 2) at different intensity levels. The slope of the best linear fit (solid line) is 0.825 ± 0.032 .

fractal dimensions were converted to 3D fractal dimensions using results from previous studies. For the distribution of point objects (stars, HII regions and GMCs) we used the results for projected disks derived in Sánchez & Alfaro (2008, Fig. 1) assuming a flatness (that is, a disk thickness to diameter ratio) of 10^{-2} (Ma et al. 1998). For the CO map we used the results obtained in Sánchez et al. (2005) with a “resolution” (i.e. the maximum distance in the image in pixel units) of $N_{pix} \sim 200$ pixels. In any case, the corresponding 3D fractal dimension for the perimeter-area dimension derived here is very weakly dependent on N_{pix} (see Fig. 8 in Sánchez et al. 2005). The procedure of estimating a 3D fractal dimension from its corresponding projected value usually increases the associated uncertainties. We have included in column labeled $D_{f,3D}$ in Table 1 the range of three-dimensional dimensions that are compatible with the calculated values of D_c or D_{per} . It is important to note, however, that these relatively large uncertainties do not arise from the method used to calculate D_f , but from possible random fluctuations in the projection of the original fractals. That is, it is not possible in principle (at least using only information from spatial distribution) to disentangle which of the projected clumps are real and which are the result of chance groupings during the projection.

4. Discussion

The first thing we note is a statistically significant difference between the projected dimensions at relatively small spatial scales and those at larger spatial scales. At small scales the correlation dimension of the distribution of stars and HII regions is $\lesssim 1.5$ whereas at large scales it is $\gtrsim 1.9$, and the differences are always larger than the associated uncertainties (Table 1). The spatial scale where this transition takes place is roughly the same for each component ($\sim 500 - 1000$ pc). The transition from a smaller correlation dimension to a larger one for the young stars in M33 was first reported by Odekon (2008). Here we provide a more detailed quantification of this transition and observe it for the first time for the distribution of HII regions. The transition is not observed for the distribution of GMCs, but given the limited number of data points for this sample ($N = 149$) the lower limit of reliable values is higher than for the other objects ($r \gtrsim 500$ pc).

What is the nature of this transition? It is not a simple edge effect. Our algorithm corrects for edge effects and, as discussed by Odekon (2008), we would expect an edge effect to cause a *decrease* in the slope on larger scales. On the other hand, some kind of change in the measured dimension is expected for projected fractal disks. Given a monofractal of three-dimensional dimension $D_{f,3D}$, the projected fractal dimension $D_{f,2D}$ of an extracted slice will depend on the slice thickness H (see Sánchez & Alfaro 2008, for detailed models and discussion). For very thin slices $D_{f,2D} = D_{f,3D} - 1$ whereas for thick slices $D_{f,2D} = \min\{2, D_{f,3D}\}$ (Falconer 1990). Then, when calculating the correlation function we should observe a change in the behavior around the scale H . For $r \gg H$ the distribution can be seen as a thin slice whereas $r \ll H$ corresponds to a very thick slice (this latter situation is analogous to a simple, direct, projection). However, this is expected to produce *smaller* values of $D_{f,2D}$ for larger spatial scales (see Fig. 1 in Sánchez & Alfaro 2008). This kind of transition has been observed in the distribution of neutral hydrogen in the LMC (Elmegreen et al. 2001) and NGC 1058 (Dutta et al. 2009a). The two-dimensional power spectra of these galaxies flattens at large scales, indicating a smaller fractal dimension; this behavior can be interpreted in terms of a change from 3D fluctuations on small scales to 2D fluctuations on scales larger than the disk thickness. In fact, power spectrum analysis has been suggested as a tool to determine the thickness of nearly face-on galactic gas layer (Elmegreen et al. 2001; Padoan et al. 2001). This effect contrasts with those presented here for molecular gas and young stars, where the correlation dimension is higher on larger scales.

A different possibility was suggested by Padoan et al. (2001). They argued that there must be a *physical* transition in the statistical properties of the flow close to the disk scale height. In turbulent flow the energy is injected at certain spatial scale and then it “cascades” to smaller scales. But there are many possible energy sources that may be relevant

at different levels—for instance, stellar outflows at small scales and galactic shear at large scales. A possible consequence may be different distribution patterns at different size ranges. Even though the underlying turbulent structure tends to be the same, non-turbulent motions acting on galactic scales could modify the final structure at those scales. In other words, the power law behavior at small spatial scales would be a direct consequence of the self-similar turbulent motions in the medium, but this turbulence is unlikely to extend to very large scales, where two-dimensional flows should dominate the dynamics. The transition from small-scale three-dimensional turbulence to two-dimensional large-scale motions on the disk should occur around the galactic scale height. Interestingly, the behavior we observe is that all the fractal dimensions at $r \gtrsim 1$ kpc are within a narrow range of values ($D_{f,2D} = 1.9 - 2.0$, or $D_{f,3D} = 2.8 - 3.0$) that are consistent with essentially uniform (random) distributions. Thus, we identify a characteristic spatial scale (around 500 – 1000 pc) that separates two different physical regimes. This scale is of the order of the typical size estimated by Efremov & Elmegreen (1998) for the largest star complexes in spiral galaxies, which correlates with the galaxy isophotal radius R_{25} (Elmegreen & Elmegreen 1983). The transition zone separates regions where coherent star formation is occurring in a turbulent medium (stellar complexes) from larger regions that are organized by large-scale galactic dynamics. The analysis of the transition in the fractal dimension provides an interesting method to determine the typical size of star complexes in a given galaxy.

Despite the rather large uncertainties for $D_{f,3D}$, it can be clearly seen that there are two separate range of results for the three-dimensional fractal structures at small spatial scales. On one hand, bright stars and molecular gas are distributed with $D_{f,3D} \lesssim 1.9$. Young, newborn stars should reflect the same conditions of the ISM from which they were formed, which is roughly consistent with this result. On the other hand, faint stars and HII regions have $D_{f,3D} \simeq 2.2 - 2.5$. These higher fractal dimension values can be interpreted in terms of evolutionary effects. The clumpy distributions of young stars in LMC (Bastian et al. 2009) and SMC (Gieles et al. 2008) evolve towards smoother distributions as stellar ages increase. The same is true for the stars clusters in these galaxies (Bonatto & Bica 2010). It has been shown that the *brightest* HII regions in spiral galaxies (which reflect, in a first approximation, the initial distribution of star-forming sites) tend to be distributed in more clumpy patterns than the low-brightness regions (Sánchez & Alfaro 2008). The higher fractal dimensions for faint stars and HII regions at small scales are probably due to this kind of evolutionary effect.

We can compare the small-scale three-dimensional structure of the interstellar medium in M33 with that of our own galaxy. The spectral index γ of the power spectrum in the Milky Way lies in the range $2.8 \lesssim \gamma \lesssim 3.2$ in 2D maps (Elmegreen & Scalo 2004). Brunt & Heyer (2002b) systematically measured the energy spectrum in several CO emission maps of the outer Galaxy and obtained $\beta = 2.17 \pm 0.31$, significantly higher than the Kolmogorov spec-

trum $\beta = 5/3 \simeq 1.67$. The corresponding dimension of the projected contours is $D_{\text{per}} \simeq 1.4$, very similar to the average value found from direct measurements of D_{per} in the Galaxy (Elmegreen & Scalo 2004). In a previous work (Sánchez et al. 2007b) we used various molecular emission maps to study the fractal properties of Ophiuchus, Perseus, and Orion, and found that the dimension is always in the range $D_{\text{per}} \simeq 1.30 - 1.35$. See Appendix A for a discussion of the definitions and relationships among γ , β , and D_{per} .

The 3D fractal dimension of the distribution of molecular gas for M33 ($D_{f,3D} \simeq 1.6 - 1.8$, Table 1), meanwhile, is much smaller than for the Milky Way ($D_{f,3D} \simeq 2.6 - 2.8$, see Sánchez et al. 2005, 2007b). The CO emission map value of $D_{\text{per}} = 1.65$ corresponds to $\beta = 1.7$, very close to the Kolmogorov value of $5/3^3$. Elmegreen et al. (2003) found, from azimuthal scans of M33, that the power spectrum of optical emission has an index even smaller than the Kolmogorov value, although the uncertainties are relatively high. That is, the boundaries of the projected perimeters in M33 are on average more irregular (higher D_{per} values) than those of the Milky Way because molecular clouds in M33 exhibit a more fragmented structure (smaller $D_{f,3D}$ values). The fact that $D_{f,3D} \lesssim 1.9$ for the three-dimensional distribution of very young stars is consistent with the small fractal dimension of the CO gas. In addition, Bastian et al. (2007), using the minimum spanning tree technique, found that the number of objects increases with the radius as $N \sim R^\alpha$ with $\alpha = 1.63 - 1.96$. Random sampling in perfect hierarchical fractals yields $N \sim R^{D_f}$ so that, in general, their results are consistent with the relatively small fractal dimensions we are reporting here. Whether there are (or not) other differences with GMCs in our Galaxy remain an open problem. Engargiola et al. (2003) found that the mass spectrum of GMCs in M33 follows a power-law distribution (according to a hierarchical picture) but with a slope considerably steeper than that found in the Milky Way. However, Sheth et al. (2008) concluded that if the same cloud identification algorithm and analysis technique are applied, and if resolution-dependent effects are taken into account, then there seem to be no differences in the GMCs properties between these two galaxies. Bolatto et al. (2008) analyzed in a consistent manner GMC properties (sizes, velocity dispersions, and luminosities) in several galaxies (including M33) subject to a wide variety of physical conditions and found only small differences with the properties of GMCs in the Milky Way. However, it is important to keep in mind the difficulty in comparing observations of an external galaxy with observations of the Milky Way. Molecular clouds from large-scale surveys in the Milky Way can be blended in space and velocity, making it troublesome to extract information on their internal structures. Blending effects are reduced in external galaxies such as M33 that are seen nearly face-on.

³This is only a reference value. We are not saying that turbulence in M33 actually behaves according to Kolmogorov’s description.

Moreover, the internal structure of GMCs in the Milky Way is measured for clouds in the solar neighborhood, at an average Galactocentric distance of about 8 kpc. Instead, the average internal structure of clouds in M33 was calculated in this work for the molecular map of the central region, at galactocentric distance less than $\sim 2 - 3$ kpc. Obviously, more detailed studies are needed to clarify this point but, in this work, we have found a significant and remarkable difference in the internal structure of GMCs between M33 and the Milky Way.

5. Conclusions

In this work we measure the clustering in the distribution of stars, HII regions, molecular gas, and individual giant molecular clouds in M33 as a function of spatial scale. We identify a transition in the clustering strength from a very clumpy (fractal) structure at relatively small scales to almost uniform patterns at larger scales. The spatial scale for this transition is in the range $\sim 500 - 1000$ pc, independently from the type of object considered. We argue that this characteristic scale separates two physical regimes, one where small-scale turbulent motions generate self-similar structures and another dominated by large-scale galactic dynamics.

The existence of this transition implies that care must be taken in calculating a single value for the fractal dimension over a large range of scales. One must take into account not only edge effects on large scales and sampling/resolution effects on small scales, but also the possibility of physical changes on intermediate scales. Ideally, this could be done using the differential form of the correlation function combined with an edge-correction algorithm; this way, changes with scale are not carried into the calculation of the dimension for larger scales. However, for small data sets (even the larger data sets presented here, with on the order of 1000 objects), the differential form is rather noisy.

At small spatial scales, bright stars and molecular gas in M33 are distributed with nearly the same three-dimensional fractal dimension. This result is consistent with the idea that newborn stars follow the same patterns of the ISM from which they were formed. Faint stars and HII regions exhibit higher fractal dimensions possibly as a consequence of evolutionary relaxation.

Interestingly, the three-dimensional fractal dimension of molecular gas in M33 ($D_{f,3D} \lesssim 1.9$) is significantly smaller than in the Milky Way ($D_{f,3D} \simeq 2.7 \pm 0.1$). This means that the interstellar medium in M33 is on average more fragmented and irregular than in our own galaxy. This result may have important implications for the study of the physical processes that determine the ISM structure.

We acknowledge Erik Rosolowsky for providing the CO emission maps of the central region of M33. We want to thank Bruce Elmegreen for helpful comments and discussion. We also thank an anonymous referee for his/her comments. This research has made use of NASA’s Astrophysics Data System and of HyperLeda and VizieR databases. We acknowledge financial support from MICINN of Spain through grant AYA2007-64052 and from Consejería de Educación y Ciencia (Junta de Andalucía) through TIC-101 and TIC-4075. N.S. is supported by a post-doctoral JAE-Doc (CSIC) contract. E.J.A. acknowledges financial support from the Spanish MICINN under the Consolider-Ingenio 2010 Program grant CSD2006-00070: “First Science with the GTC”.

A. Appendix

Interstellar turbulence can be characterized in several different ways. Two commonly used measures are the energy spectrum $E(k) \sim |k|^{-\beta}$ and the power spectrum $P(k) \sim |k|^{-\gamma}$ for wavenumber k . The energy spectrum is the integral over all directions of the power spectrum, $E(k)dk = \int P(k)d\Omega$, so that with this nomenclature the scaling exponents β and γ are related through (Brunt & Heyer 2002a)

$$\gamma = \beta + E - 1 \quad ,$$

where E is the euclidean dimension of the image. For example, for a dissipationless cascade of energy through an incompressible fluid the Kolmogorov energy spectrum is $\beta = 5/3$ and the power spectrum index is $\gamma = 11/3, 8/3, \text{ or } 5/3$ in 3D, 2D or 1D, respectively (Elmegreen & Scalo 2004).

The structure of molecular clouds can also be described as a fractional Brownian motion (fBm) structure (Stutzki et al. 1998; Miville-Deschênes et al. 2003). The properties of fBm clouds depend on a single parameter, the so-called Hurst exponent H . This parameter characterizes the self-similar structure and it is related to the corresponding power spectrum through (Miville-Deschênes et al. 2003)

$$\gamma = 2H + E \quad .$$

The iso-intensity contours of the E -dimensional image of a fBm-cloud is given by $D_{\text{iso}} = E - H$ (Stutzki et al. 1998), which corresponds to the perimeter-area based dimension D_{per} for two-dimensional maps. In this last case ($E = 2$) we can write the equations relating these commonly used parameters as

$$D_{\text{per}} = 2 - H \quad ,$$

$$D_{\text{per}} = (5 - \beta)/2 \quad ,$$

and

$$D_{\text{per}} = (6 - \gamma)/2 \quad .$$

For very rough structures ($H = 0$), we have $\beta = 1$, $\gamma = 2$ and $D_{\text{per}} = 2$, while for very smooth structures ($H = 1$) we get $\beta = 3$, $\gamma = 4$ and $D_{\text{per}} = 1$.

REFERENCES

- Allison, R. J., Goodwin, S. P., Parker, R. J., de Grijs, R., Portegies Zwart, S. F., & Kouwenhoven, M. B. N. 2009, *ApJ*, 700, L99
- Bastian, N., Ercolano, B., Gieles, M., Rosolowsky, E., Scheepmaker, R. A., Gutermuth, R., & Efremov, Y. 2007, *MNRAS*, 379, 1302
- Bastian, N., Gieles, M., Ercolano, B., & Gutermuth, R. 2009, *MNRAS*, 392, 868
- Bergin, E. A., & Tafalla, M. 2007, *ARA&A*, 45, 339
- Bolatto, A. D., Leroy, A. K., Rosolowsky, E., Walter, F., & Blitz, L. 2008, *ApJ*, 686, 948
- Bonanos, A. Z., et al. 2006, *ApJ*, 652, 313
- Bonatto, C., & Bica, E. 2010, *MNRAS*, 403, 996
- Brunt, C. M., & Heyer, M. H. 2002a, *ApJ*, 566, 276
- Brunt, C. M., & Heyer, M. H. 2002b, *ApJ*, 566, 289
- Burkert, A. 2006, *Comptes Rendus Physique*, 7, 433
- Cartwright, A., & Whitworth, A. P. 2004, *MNRAS*, 348, 589
- Curtis, E. I., & Richer, J. S. 2010, *MNRAS*, 402, 603
- de La Fuente Marcos, R., & de La Fuente Marcos, C. 2006, *A&A*, 452, 163
- de la Fuente Marcos, R., & de la Fuente Marcos, C. 2009, *ApJ*, 700, 436
- Dutta, P., Begum, A., Bharadwaj, S., & Chengalur, J. N. 2008, *MNRAS*, 384, L34
- Dutta, P., Begum, A., Bharadwaj, S., & Chengalur, J. N. 2009a, *MNRAS*, 397, L60
- Dutta, P., Begum, A., Bharadwaj, S., & Chengalur, J. N. 2009b, *MNRAS*, 398, 887

- Efremov, Y. N. 1995, *AJ*, 110, 2757
- Efremov, Y. N., & Elmegreen, B. G. 1998, *MNRAS*, 299, 588
- Elmegreen, B. G. 2010, *IAU Symposium*, 266, 3 (arXiv:0910.4638)
- Elmegreen, B. G., & Elmegreen, D. M. 1983, *MNRAS*, 203, 31
- Elmegreen, B. G., & Falgarone, E. 1996, *ApJ*, 471, 816
- Elmegreen, B. G., Kim, S., & Staveley-Smith, L. 2001, *ApJ*, 548, 749
- Elmegreen, B. G., Leitner, S. N., Elmegreen, D. M., & Cuillandre, J.-C. 2003, *ApJ*, 593, 333
- Elmegreen, B. G., & Scalo, J. 2004, *ARA&A*, 42, 211
- Engargiola, G., Plambeck, R. L., Rosolowsky, E., & Blitz, L. 2003, *ApJS*, 149, 343
- Falconer, K. J. 1990, *Fractal Geometry: Mathematical Foundations and Applications* (London: Wiley)
- Federrath, C., Klessen, R. S., & Schmidt, W. 2009, *ApJ*, 692, 364
- Gieles, M., Bastian, N., & Ercolano, B. 2008, *MNRAS*, 391, L93
- Goodwin, S. P., & Whitworth, A. P. 2004, *A&A*, 413, 929
- Hodge, P. W., Balsley, J., Wyder, T. K., & Skelton, B. P. 1999, *PASP*, 111, 685
- Kim, S., & Park, C. 2007, *ApJ*, 663, 244
- Lada, C. J., & Lada, E. A. 2003, *ARA&A*, 41, 57
- Ma, J., Peng, Q.-H., & Gu, Q.-S. 1998, *A&AS*, 130, 449
- Massey, P., Olsen, K. A. G., Hodge, P. W., Strong, S. B., Jacoby, G. H., Schlingman, W., & Smith, R. C. 2006, *AJ*, 131, 2478
- Mac Low, M.-M., & Klessen, R. S. 2004, *Reviews of Modern Physics*, 76, 125
- McKee, C. F., & Ostriker, E. C. 2007, *ARA&A*, 45, 565
- Miville-Deschênes, M.-A., Levrier, F., & Falgarone, E. 2003, *ApJ*, 593, 831
- Odekon, M. C. 2006, *AJ*, 132, 1834
- Odekon, M. C. 2008, *ApJ*, 681, 1248

- Padoan, P., Kim, S., Goodman, A., & Staveley-Smith, L. 2001, *ApJ*, 555, L33
- Parodi, B. R., & Binggeli, B. 2003, *A&A*, 398, 501
- Pineda, J. E., Rosolowsky, E. W., & Goodman, A. A. 2009, *ApJ*, 699, L134
- Rosolowsky, E., Keto, E., Matsushita, S., & Willner, S. P. 2007, *ApJ*, 661, 830
- Sánchez, N., Alfaro, E. J., & Pérez, E. 2005, *ApJ*, 625, 849
- Sánchez, N., Alfaro, E. J., & Pérez, E. 2006, *ApJ*, 641, 347
- Sánchez, N., Alfaro, E. J., Elias, F., Delgado, A. J., & Cabrera-Caño, J. 2007a, *ApJ*, 667, 213
- Sánchez, N., Alfaro, E. J., & Pérez, E. 2007b, *ApJ*, 656, 222
- Sánchez, N., & Alfaro, E. J. 2008, *ApJS*, 178, 1
- Sánchez, N., & Alfaro, E. J. 2009, *ApJ*, 696, 2086
- Scheepmaker, R. A., Lamers, H. J. G. L. M., Anders, P., & Larsen, S. S. 2009, *A&A*, 494, 81
- Schmeja, S., & Klessen, R. S. 2006, *A&A*, 449, 151
- Schmeja, S., Kumar, M. S. N., & Ferreira, B. 2008, *MNRAS*, 389, 1209
- Schneider, N., Bontemps, S., Simon, R., Ossenkopf, V., Federrath, C., Klessen, R., Motte, F., & Brunt, C. 2010, arXiv:1001.2453
- Sheth, K., Vogel, S. N., Wilson, C. D., & Dame, T. M. 2008, *ApJ*, 675, 330
- Shetty, R., Collins, D. C., Kauffmann, J., Goodman, A. A., Rosolowsky, E. W., & Norman, M. L. 2010, *ApJ*(in press, arXiv:1001.4549)
- Stanimirovic, S., Staveley-Smith, L., Dickey, J. M., Sault, R. J., & Snowden, S. L. 1999, *MNRAS*, 302, 417
- Stutzki, J., Bensch, F., Heithausen, A., Ossenkopf, V., & Zielinsky, M. 1998, *A&A*, 336, 697
- U, V., Urbaneja, M. A., Kudritzki, R.-P., Jacobs, B. A., Bresolin, F., & Przybilla, N. 2009, *ApJ*, 704, 1120
- Willett, K. W., Elmegreen, B. G., & Hunter, D. A. 2005, *AJ*, 129, 2186

